J. Appl. Comput. Mech., 12(3) (2026) 1217-1232
DOI: 10.22055/jacm.2026.48980.5640

ISSN: 2383-4536
jacm.scu.ac.ir

Shahid Chamran
University of Ahvaz

Journal of
Applied and Computational Mechanics

Research Paper

Nonlocal Static and Dynamic Characterization of Nanobeams on Elastic Substrates with Surface Energy Effects

Worathep Sae-Long[1], Suchart Limkatanyu[2], Piti Sukontasukkul[3], Jaroon Rungamornrat[4,5], Suraparb Keawsawasvong[6], Thanakorn Chompoorat[1], Preeda Chaimahawan[1], Amorn Pimanmas[7]

[1] Civil Engineering Program, School of Engineering, University of Phayao, Phayao, 56000, Thailand,
Email: worathep.sa@up.ac.th (W.S.-L.); thanakorn.ch@up.ac.th (T.C.); preeda.ch@up.ac.th (P.C.)

[2] Department of Civil and Environmental Engineering, Faculty of Engineering, Prince of Songkla University, Songkhla, 90110, Thailand, Email: suchart.l@psu.ac.th

[3] Construction and Building Materials Research Center, Department of Civil Engineering, King Mongkut's University of Technology North Bangkok, Bangkok, 10800, Thailand, Email: piti.s@eng.kmutnb.ac.th

[4] Center of Excellence in Applied Mechanics and Structures, Department of Civil Engineering, Faculty of Engineering, Chulalongkorn University, Bangkok 10330, Thailand, Email: jaroon.r@chula.ac.th

[5] GreenTech Nexus: Research Center for Sustainable Construction Innovation, Faculty of Engineering, Chulalongkorn University, Bangkok 10330, Thailand

[6] Research Unit in Sciences and Innovative Technologies for Civil Engineering Infrastructures, Department of Civil Engineering, Faculty of Engineering, Thammasat School of Engineering, Thammasat University, Pathumthani, 12120, Thailand, Email: ksurapar@engr.tu.ac.th

[7] Department of Civil Engineering, Kasetsart University, Bangkok, 10900, Thailand, Email: amorn.pi@ku.ac.th

Received December 06 2025; Revised January 27 2026; Accepted for publication March 25 2026.
✉ Corresponding author: S. Limkatanyu (suchart.l@psu.ac.th)

Abstract. This study proposes a unified beam–substrate model for the static and dynamic characterization of nanobeams resting on elastic substrates, explicitly incorporating size-dependent surface energy effects. The formulation combines the modified strain gradient elasticity theory (MSGET) with the Euler–Bernoulli beam theory to capture nonclassical bulk behavior through three intrinsic length-scale parameters, while the substrate–structure interaction is modeled using a Winkler foundation. Surface energy effects are incorporated via the Gurtin–Murdoch surface elasticity framework. Hamilton's principle is used to derive the governing equation of motion and the associated boundary conditions, from which closed-form solutions are obtained for bending, buckling, and free vibration. Representative simulations demonstrate pronounced stiffening induced by the combined effects of MSGET nonlocality, surface energy, and foundation stiffness. For the cantilever case, the proposed model predicts a tip-deflection reduction of approximately 64.14% compared with the classical local model. For simply supported systems, the normalized critical buckling load and the normalized first natural frequency can reach up to 27.05 and 5.17, respectively, over the considered parameter ranges. These findings underscore the importance of accounting for small-scale and surface effects in the design and interpretation of the mechanical response of nanobeam–substrate systems.

Keywords: Euler-Bernoulli beam, Bending analysis, Buckling analysis, Free vibration analysis, Modified strain gradient theory.

1. Introduction

Recent technological advancements have driven numerous scientific and engineering innovations [1–2]. Among these, nanoscale technologies have attracted increasing attention due to their broad impact on engineering applications. Representative examples include nanowires [3], nanoscale actuators [4], nanoscale sensors [5], and atomic force microscopes (AFM) [6]. Accordingly, understanding the structural behavior of nanoscale materials is essential to ensure their strength and reliability, which motivates the present study. In studies of nanostructural behavior [7–13], experimental results are generally regarded as more reliable than theoretical predictions. Nevertheless, nanoscale experimental investigations face major challenges, such as the need for specialized equipment, high cost, and technological limitations [7–8]. Consequently, mathematical modeling remains a widely used and effective approach for analyzing the mechanical behavior of nanostructures [9–13].

Typically, micro- and nanostructures are modeled using three main approaches: atomistic models [14–15], continuum models [16–19], and hybrid frameworks that couple atomistic and continuum mechanics [20–21]. Atomistic and hybrid approaches are less commonly used than continuum models because their discrete description of matter and inherent complexity generally require longer computational times and substantially higher computational cost [14, 15, 20, 21]. As a result, continuum modeling is widely regarded as an effective alternative that offers a practical balance between accuracy and simplicity [16–19]. To date, non-classical

Published online: March 30 2026

continuum models, often combined with higher-order elasticity theories, have been extensively developed and applied to investigate the static and dynamic mechanical behavior of micro- and nanostructures [22–30].

Among higher-order elasticity theories, the modified strain gradient elasticity theory (MSGET), originally introduced by Lam et al. [7], incorporates three material length-scale parameters to represent the discrete nature of matter in nanostructures. In addition to the conventional equilibrium of forces and moments, the theory also accounts for the equilibrium of couple-stress moments. Consequently, MSGET has proved to be a powerful tool for investigating the mechanical behavior of nanostructures over the past two decades [31–38]. For example, Movassagh and Mahmoodi [31] employed MSGET to refine the classical plate model and study size effects in microscale Kirchhoff plates under static loading. Ansari et al. [32] applied MSGET to curved microbeams made of functionally graded (FG) materials, developing a beam formulation that includes small-scale effects and first-order shear deformation. They subsequently extended this framework to circular and annular FG microplates to examine axisymmetric bending, buckling, and free vibration [33]. Salehipour and Shahsavar [34] and Thai et al. [35] used MSGET-based plate models to analyze size-dependent static and free-vibration responses of FG micro/nanoplates. Bostani and Mohammadi [36] investigated size effects on the quality factor associated with thermoelastic damping in microbeam resonators by combining MSGET with the Lord–Shulman theory for silicon microbeams in cantilever and clamped–clamped configurations. Su et al. [37] studied the nonlinear behavior of porous FG composite rectangular microplates with and without cutouts, while Chu et al. [38] examined nonlinear free vibrations of PFG composite microplates and assessed how microstructural tensors influence large-amplitude oscillations. Overall, these studies [31–38] demonstrate MSGET's strong capability to capture size-dependent responses in micro- and nanostructures. Accordingly, MSGET is adopted in the present work to investigate size-scale effects within the proposed model.

In addition to size-scale effects, free surface energy becomes increasingly important as structural dimensions decrease. This behavior arises from the energy difference between the free surface and the bulk material, which can introduce pronounced size-dependent characteristics in nanoscale structures. To capture this phenomenon, Gurtin and Murdoch [39, 40] proposed the surface continuum model, building on and modifying Cammarata's surface elasticity theory [41]. Because this model can be incorporated into continuum formulations in a relatively straightforward manner, it has been widely used to study surface effects in nanoscale structures [42–48]. Prior studies [42–48] have shown that the Gurtin–Murdoch surface model can effectively represent such size-dependent influences; therefore, it is adopted in the present work.

Over the past two decades, the concept of beams on elastic foundations has been widely employed to develop and analyze the interaction behavior between nanoscale structures and elastic support layers [9, 11, 16, 18, 22]. These studies have contributed to nanoscale innovations, including stretchable electronics [49–50], flexible optoelectronics [51], and carbon nanotube-reinforced composites (CNTRCs) [52–53]. Despite these advances, reliable and accurate mathematical models for nanobeams on elastic substrates are still needed and remain an active area of research [16, 18, 29, 45, 55–59]. For instance, Limkatanyu et al. [16] utilized Eringen's nonlocal elasticity framework to enhance a beam–substrate model for examining the flexural behavior of nanobeams. Sae-Long et al. [18] further advanced this framework by analyzing the buckling and flexural responses of nanobeams within the context of the thermodynamics-based strain gradient theory [54]. Limkatanyu et al. [45] also developed a modified strain-gradient elasticity model to account for small-scale effects in nanobeams on elastic substrates. Rezaee and Hamidi [55] examined nonlinear vibrations of nanobeams on viscoelastic media using nonlocal elasticity theory to address material and geometric nonlinearities. Mamu and Togun [56] employed a perturbation method to study Euler–Bernoulli nanobeam vibrations under thermal effects, including Winkler, Pasternak, and nonlinear foundation interactions. Zhang et al. [57] proposed a viscoelastic nanobeam model with axial pretension embedded in an elastic substrate, using the Kelvin viscoelastic model. Civalek et al. [29] investigated functionally graded nanobeams with nonlocal strain gradient theory, incorporating elastic springs at the ends for stability analysis. Uzun and Yaylı [58] examined the buckling response of nanoscale beams supported by a one-parameter elastic foundation using the nonlocal strain gradient elasticity theory. Finally, Limkatanyu et al. [59] utilized a mixed stress-driven nonlocal formulation to integrate both surface-energy and nonlocality effects into the beam–substrate interaction system. Their study demonstrated that substrate–structure interactions, surface energy, and material nonlocality significantly influence the flexural behavior of nanobeams. Although numerous beam–foundation formulations have been developed for nanoscale applications [16, 18, 29, 45, 55–59], most existing models incorporate either nonlocal/strain-gradient effects in the bulk or surface elasticity effects, whereas only a limited number account for both within a single framework for nanobeams resting on elastic substrates. In particular, to the best of the authors' knowledge, MSGET (with three independent material length-scale parameters) has not yet been coupled with the Gurtin–Murdoch surface elasticity model in a beam–substrate system to provide a unified analytical treatment of bending, buckling, and free vibration. Accordingly, further development of beam–substrate medium models is needed to capture size-dependent effects in nanostructures and to enable accurate analysis of flexural response, buckling, and free vibration. The present work addresses this gap by developing an integrated formulation and presenting closed-form solutions together with systematic parametric investigations.

The central aim of this research is to formulate an integrated model that couples nanobeams with a substrate medium, enabling a unified investigation of the flexural, buckling, and free-vibration characteristics of nanobeam–substrate systems. The proposed model combines the MSGET, Winkler foundation model [60], Euler–Bernoulli beam theory (EBBT), and Gurtin–Murdoch surface model. This represents the first application of these theories and models together in a nanobeam–substrate system, highlighting the novelty of the present work compared with previous studies [16, 18, 29, 45, 55–59]. The schematic configuration of the proposed approach is illustrated in Fig. 1. The methodology begins with model formulation, including kinematic assumptions, MSGET, nanobeam–substrate interactions, and surface elasticity theory. The model is then applied to evaluate bending, buckling, and free vibration responses, as presented in the numerical simulations section. All simulations were performed using Mathematica [61].

2. Kinematic Assumptions of the Nanobeam

The kinematic assumptions of the nanobeam in this study are based on EBBT [62], which states that the beam cross-section remains plane and perpendicular to the longitudinal axis during deformation. According to these assumptions, the displacement fields can be expressed as:

$$X(x,z) = -z\frac{\partial w(x)}{\partial x};\ Y(x,z) = 0;\ \text{and}\ \ Z(x,z) = w(x) \tag{1}$$

where $X(x,z)$, $Y(x,z)$, and $Z(x,z)$ denote the displacements along the x-, y-, and z-axes, respectively; z represents the transverse distance measured from the x-axis; and $w(x)$ is the transverse displacement of the nanobeam section.

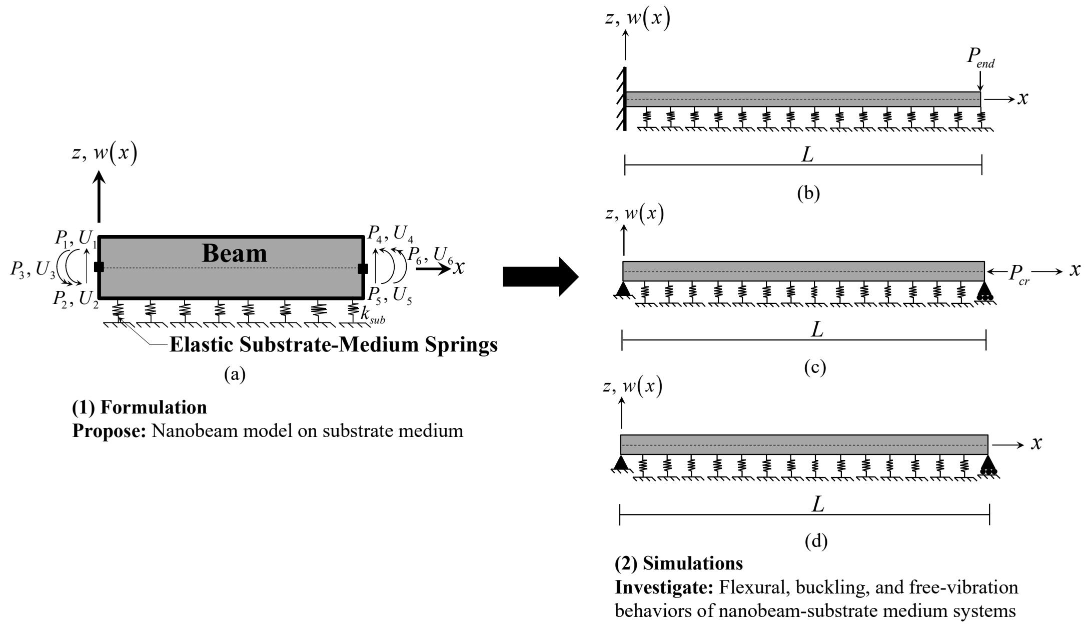

Fig. 1. Schematic illustration of the proposed nanobeam–substrate medium model and the boundary conditions adopted in the numerical simulations: (a) beam-foundation element, (b) flexural analysis, (c) buckling analysis, and (d) free-vibration analysis.

3. Modified Strain Gradient Elasticity Theory (MSGET)

In 2003, Lam et al. [7] proposed the MSGET, which introduces higher-order equilibrium equations to describe the behavior associated with higher-order stresses. Beyond the traditional equilibrium conditions for forces and moments, MSGET additionally enforces the equilibrium of couple-stress moments [7, 63]. For isotropic linear elastic materials, the constitutive framework comprises three independent higher-order material length-scale parameters in addition to the two classical elastic constants. The strain energy (*U*) of an isotropic linear elastic solid occupying the volume (*V*) is formulated as follows:

$$U = \frac{1}{2}\int_V \left(\sigma_{ij}\varepsilon_{ij} + p_i\gamma_i + \tau^{(1)}_{ijk}\eta^{(1)}_{ijk} + m^{(s)}_{ij}\chi^{(s)}_{ij}\right)dV \tag{2}$$

where σ_{ij} is the Cauchy stress tensor; ε_{ij} is the strain tensor; p_i, $\tau^{(1)}_{ijk}$, and $m^{(s)}_{ij}$ represent higher-order stress tensors; γ_i, $\eta^{(1)}_{ijk}$, and $\chi^{(s)}_{ij}$ are the corresponding strain-gradient measures; and denotes the material volume.

The deformation measures can be expressed mathematically as follows [63]:

$$\varepsilon_{ij} = \frac{1}{2}\left(\mathbf{u}_{i,j} + \mathbf{u}_{j,i}\right) \tag{3}$$

$$\gamma_i = \varepsilon_{mm,i} \tag{4}$$

$$\eta^{(s)}_{ijk} = \frac{1}{3}\left(\varepsilon_{jk,i} + \varepsilon_{ki,j} + \varepsilon_{ij,k}\right) - \frac{1}{15}\delta_{ij}\left(\varepsilon_{mm,k} + 2\varepsilon_{mk,m}\right) - \frac{1}{15}\left[\delta_{jk}\left(\varepsilon_{mm,i} + 2\varepsilon_{mi,m}\right) + \delta_{ki}\left(\varepsilon_{mm,j} + 2\varepsilon_{mj,m}\right)\right] \tag{5}$$

$$\chi^{(s)}_{ij} = \frac{1}{2}\left(e_{ipq}\varepsilon_{qj,p} + e_{jpq}\varepsilon_{qi,p}\right) \tag{6}$$

where $\mathbf{u}_i$ denotes the displacement vector; e_{ijk} denotes the permutation symbol; and δ_{ij} denotes the Kronecker delta.

The constitutive stress–strain relationships within the framework of the MSGET [7] can be formulated as follows:

$$\sigma_{ij} = k\delta_{ij}\varepsilon_{mm} + 2\mu\varepsilon'_{ij} \tag{7}$$

$$p_i = 2\mu l_0^2\gamma_i \tag{8}$$

$$\tau^{(1)}_{ijk} = 2\mu l_1^2\eta^{(1)}_{ijk} \tag{9}$$

$$m^{(s)}_{ij} = 2\mu l_2^2\chi^{(s)}_{ij} \tag{10}$$

with

$$\varepsilon'_{ij} = \varepsilon_{ij} - \frac{1}{3}\varepsilon_{mm}\delta_{ij} \tag{11}$$

where μ and k denote the shear modulus and bulk modulus, respectively; l_0, l_1, and l_2 represent the additional material length-scale parameters associated with dilatation gradients, deviatoric stretch gradients, and rotation gradients, respectively; and ε'_{ij} denotes the deviatoric strain.

Based on the EBBT, as described in Eq. (1), the non-zero strain measures in Eqs. (3) to (6) can be expressed as follows:

$$\varepsilon_{xx}(x,t) = -z\frac{\partial^2 w(x,t)}{\partial x^2} \tag{12}$$

$$\gamma_x(x,t) = -z\frac{\partial^3 w(x,t)}{\partial x^3} \text{ and } \gamma_z(x,t) = -\frac{\partial^2 w(x,t)}{\partial x^2} \tag{13}$$

$$\eta^{(1)}_{xxx}(x,t) = -\frac{2}{5}z\frac{\partial^3 w(x,t)}{\partial x^3} \tag{14}$$

$$\eta^{(1)}_{xxz}(x,t) = \eta^{(1)}_{xzx}(x,t) = \eta^{(1)}_{zxx}(x,t) = -\frac{4}{15}\frac{\partial^2 w(x,t)}{\partial x^2} \tag{15}$$

$$\eta^{(1)}_{xyy}(x,t) = \eta^{(1)}_{yyx}(x,t) = \eta^{(1)}_{yxy}(x,t) = \eta^{(1)}_{xzz}(x,t) = \eta^{(1)}_{zzx}(x,t) = \eta^{(1)}_{zxz}(x,t) = \frac{1}{5}z\frac{\partial^3 w(x,t)}{\partial x^3} \tag{16}$$

$$\eta^{(1)}_{yyz}(x,t) = \eta^{(1)}_{yzy}(x,t) = \eta^{(1)}_{zyy}(x,t) = \frac{1}{15}\frac{\partial^2 w(x,t)}{\partial x^2} \tag{17}$$

$$\eta^{(1)}_{zzz}(x,t) = \frac{1}{5}\frac{\partial^2 w(x,t)}{\partial x^2} \tag{18}$$

$$\chi^{(s)}_{xy}(x,t) = \chi^{(s)}_{yx}(x,t) = -\frac{1}{2}\frac{\partial^2 w(x,t)}{\partial x^2} \tag{19}$$

For the present Euler–Bernoulli nanobeam model, Poisson coupling is neglected, and the dominant axial stress is represented by $\sigma_{xx}(x,t) = E_{xx}\varepsilon_{xx}(x,t)$. This assumption is consistent with the classical one-dimensional beam idealization for slender beams with traction-free lateral surfaces, in which $\sigma_{xx}(x,t)$ governs bending while lateral normal stresses remain negligible [16, 18]. Within the MSGET-based formulation, including Poisson's effect would primarily modify the effective constitutive coefficients appearing in the stiffness resultants; however, it would not alter the spatial order of the governing equation, which remains sixth order due to the strain-gradient measures. Accordingly, the present assumption enables a compact closed-form formulation while retaining the key size-dependent mechanisms. Its influence is expected to be most pronounced for materials with relatively large Poisson's ratios and/or for moderately thick beams, which may be addressed in future extensions.

Accordingly, under the Euler–Bernoulli beam assumptions with Poisson's effect neglected, the nonzero stress components can be reformulated, using the compatibility relations in Eqs. (12) to (19) together with the constitutive equations in Eqs. (7) to (10), as follows:

$$\sigma_{xx}(x,t) = -zE_{xx}\frac{\partial^2 w(x,t)}{\partial x^2} \tag{20}$$

$$p_x(x,t) = -2\mu l_0^2 z\frac{\partial^3 w(x,t)}{\partial x^3} \tag{21}$$

$$p_z(x,t) = -2\mu l_0^2\frac{\partial^2 w(x,t)}{\partial x^2} \tag{22}$$

$$\tau^{(1)}_{xxx}(x,t) = -\frac{4}{5}\mu l_1^2 z\frac{\partial^3 w(x,t)}{\partial x^3} \tag{23}$$

$$\tau^{(1)}_{xxz}(x,t) = \tau^{(1)}_{xzx}(x,t) = \tau^{(1)}_{zxx}(x,t) = -\frac{8}{15}\mu l_1^2\frac{\partial^2 w(x,t)}{\partial x^2} \tag{24}$$

$$\tau^{(1)}_{xyy}(x,t) = \tau^{(1)}_{yyx}(x,t) = \tau^{(1)}_{yxy}(x,t) = \tau^{(1)}_{xzz}(x,t) = \tau^{(1)}_{zzx}(x,t) = \tau^{(1)}_{zxz}(x,t) = \frac{2}{5}\mu l_1^2 z\frac{\partial^3 w(x,t)}{\partial x^3} \tag{25}$$

$$\tau^{(1)}_{yyz}(x,t) = \tau^{(1)}_{yzy}(x,t) = \tau^{(1)}_{zyy}(x,t) = \frac{2}{15}\mu l_1^2\frac{\partial^2 w(x,t)}{\partial x^2} \tag{26}$$

$$\tau^{(1)}_{zzz}(x,t) = \frac{2}{5}\mu l_1^2\frac{\partial^2 w(x,t)}{\partial x^2} \tag{27}$$

$$m^{(s)}_{xy}(x,t) = m^{(s)}_{yx}(x,t) = -\mu l_2^2\frac{\partial^2 w(x,t)}{\partial x^2} \tag{28}$$

where E_{xx} denotes the nanobeam's elastic bulk modulus.

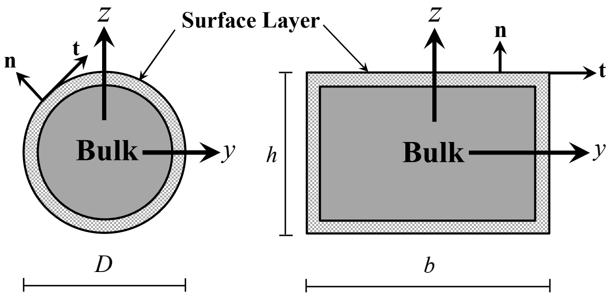

Fig. 2. Gurtin–Murdoch surface elasticity idealization: bulk core surrounded by a zero-thickness surface layer carrying surface stress [45].

4. Nanobeam-Substrate Medium Interaction

This study adopts the classical beam-on-elastic-foundation model introduced by Winkler [60] to characterize the nanobeam-substrate medium interaction. In this formulation, the substrate is idealized as a continuous distribution of independent springs along the beam's length. Consequently, the substrate medium's interaction force $(D_{sub}(x,t))$ can be expressed as follows:

$$D_{sub}(x,t) = k_{sub}\Delta_{sub}(x,t) \tag{29}$$

where k_{sub} denotes a constant of the substate medium modulus; and $\Delta_{sub}(x,t)$ denotes the substrate medium's deformation.

The Winkler foundation model [60] assumes perfect compatibility between the substrate medium and the nanobeam. Accordingly, the substrate medium's deformation $(\Delta_{sub}(x,t))$ and the nanobeam's displacement $(w(x,t))$ are related as follows:

$$\Delta_{sub}(x,t) = w(x,t) \tag{30}$$

By substituting the compatibility condition of the substrate medium from Eq. (30) into Eq. (29), the following expression is obtained:

$$D_{sub}(x,t) = k_{sub}w(x,t) \tag{31}$$

5. Surface Elasticity Theory

When structural dimensions are reduced to the nanometer scale, the contribution of surface energy becomes significant and cannot be neglected. This surface energy, analogous to the stored energy within the bulk material, begins to noticeably influence the mechanical behavior of nanoscale structures, as supported by experimental and numerical findings [39–48]. To incorporate this size-dependent effect, the proposed model adopts the Gurtin–Murdoch framework [39–40]. According to the surface elasticity hypothesis [39–40], the beam cross-section is composed of a central core surrounded by a thin outer surface layer, as depicted in Fig. 2. The model assumes a perfect bond between the core and the surrounding surface layer. The mechanical behavior of the surface layer, idealized as a mathematically thin elastic membrane with negligible thickness, is governed by its constitutive relations:

$$\tau_{ij}^{sur} = \left[\tau_{res}^{sur} + \left(\lambda^{sur} + \mu^{sur}\right)u_{m,m}^{sur}\right]\delta_{ij} + \mu^{sur}\left(u_{i,j}^{sur} + u_{j,i}^{sur}\right) - \tau_{res}^{sur}u_{j,i}^{sur} \tag{32}$$

$$\tau_{ni}^{sur} = \tau_{res}^{sur}u_{n,i}^{sur} \tag{33}$$

where τ_{ni}^{sur} and τ_{ij}^{sur} represent the out-of-plane and in-plane surface stresses, respectively; λ^{sur} and μ^{sur} denote the surface elastic constants; u^{sur} represents the surface deformation; and τ_{res}^{sur} represents the residual surface stress, as determined from atomistic simulation results [64].

For the in-plane Euler–Bernoulli beam system, the non-zero surface stresses can be expressed as described by Limkatanyu et al. [16, 45] and Guo and Mahmoud [65]:

$$\tau_{xx}^{sur}(x,t) - \tau_{res}^{sur} = E_{xx}^{sur}\varepsilon_{xx}^{sur}(x,t) \tag{34}$$

$$\tau_{nx}^{sur}(x,t) = \tau_{res}^{sur}\varepsilon_{nx}^{sur}(x,t) \tag{35}$$

where $\varepsilon_{xx}^{sur}(x)$ is the surface strain; $\tau_{xx}^{sur}(x)$ is the surface stress at the in-plane component; $E_{xx}^{sur} = \lambda^{sur} + 2\mu^{sur}$ denotes the surface elastic modulus; $\varepsilon_{nx}^{sur}(x)$ is the surface deformation; and $\tau_{nx}^{sur}(x)$ is the surface stress at the out-of-plane component.

Based on the surface model proposed by Gurtin and Murdoch [39–40], which assumes perfect bonding between the outer surface layer and the bulk core, the deformation of the surface layer and its relation to the nanobeam's transverse displacement $(w(x,t))$ can be written as follows:

$$\varepsilon_{xx}^{sur}(x,t) = -z\frac{\partial^2 w(x,t)}{\partial x^2} \tag{36}$$

$$\varepsilon_{nx}^{sur}(x,t) = n_z\frac{\partial w(x,t)}{\partial x} \tag{37}$$

where n_z represents the z-component of the unit vector **n** perpendicular to the lateral surface of the beam cross-section.

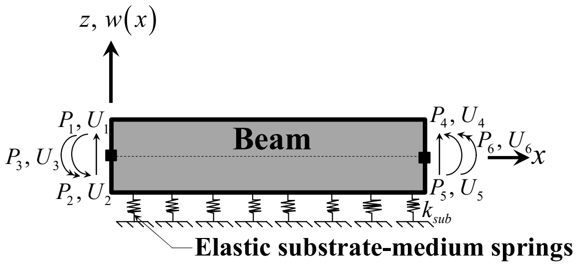

Fig. 3. Nanobeam on Winkler foundation showing the end nodal forces and nodal displacements.

By substituting the surface-layer compatibility conditions from Eqs. (36) to (37) into Eqs. (34) to (35), the following expressions are obtained:

$$\tau_{xx}^{sur}(x,t)-\tau_{res}^{sur}=-zE_{xx}^{sur}\frac{\partial^2 w(x,t)}{\partial x^2} \tag{38}$$

$$\tau_{nx}^{sur}(x,t)=n_z\tau_{res}^{sur}\frac{\partial w(x,t)}{\partial x} \tag{39}$$

6. Formulation: Hamilton's Principle

For the nanobeam–substrate medium system, the strain energy (U), incorporating the surface-energy effect (Fig. 3) for an isotropic and linearly elastic material, can be expressed mathematically as:

$$U=\frac{1}{2}\int_0^L(EI)_{eff}^L\left(\frac{\partial^2 w(x,t)}{\partial x^2}\right)^2dx+\frac{1}{2}\int_0^L(EI)_{eff}^H\left(\frac{\partial^3 w(x,t)}{\partial x^3}\right)^2dx+\frac{1}{2}\int_0^L(K)_{eff}^L\left(\frac{\partial w(x,t)}{\partial x}\right)^2dx+\frac{1}{2}\int_0^L k_{sub}\left(w(x,t)\right)^2dx \tag{40}$$

where $(EI)_{eff}^L=E_{xx}I+E_{xx}^{sur}I_\Gamma+2\mu Al_0^2+8\mu Al_1^2/15+\mu Al_2^2$ represents the lower-order flexural rigidity; $(EI)_{eff}^H=2\mu Il_0^2+4\mu Il_1^2/5$ represents the higher-order flexural rigidity; $(K)_{eff}^L=\tau_{res}^{sur}S_\Gamma-P$ represents the lower-order stiffness of the nanobeam–substrate medium system; Γ denotes the nanobeam section perimeter; L denotes the nanobeam length, denotes the applied axial force; $I_\Gamma=\oint_\Gamma z^2\,d\Gamma$ denotes the second moment of the perimeter; $I=\int_A z^2dA$ denotes the second moment of area; and $S_\Gamma=\oint_\Gamma n_z^2d\Gamma$.

By evaluating the first variation of Eq. (40) over the time interval $[0,T]$, the following expression is obtained:

$$\begin{aligned}\delta U=\int_0^T\Bigg[&\int_0^L(EI)_{eff}^L\left(\frac{\partial^2 w(x,t)}{\partial x^2}\right)\left(\frac{\partial^2\delta w(x,t)}{\partial x^2}\right)dx+\int_0^L(EI)_{eff}^H\left(\frac{\partial^3 w(x,t)}{\partial x^3}\right)\left(\frac{\partial^3\delta w(x,t)}{\partial x^3}\right)dx\\&+\int_0^L(K)_{eff}^L\left(\frac{\partial w(x,t)}{\partial x}\right)\left(\frac{\partial\delta w(x,t)}{\partial x}\right)dx+\int_0^L k_{sub}\left(w(x,t)\right)\left(\delta w(x,t)\right)dx\Bigg]dt\end{aligned} \tag{41}$$

Next, integration by parts is used to transfer the differential operators, allowing Eq. (41) to be rewritten as:

$$\begin{aligned}\delta U=&\int_0^T\left[\int_0^L\delta w(x,t)\left[-(EI)_{eff}^H\frac{\partial^6 w(x,t)}{\partial x^6}+(EI)_{eff}^L\frac{\partial^4 w(x,t)}{\partial x^4}-(K)_{eff}^L\frac{\partial^2 w(x,t)}{\partial x^2}+k_{sub}w(x,t)\right]dxdt\right.\\&+\int_0^T\delta w(x,t)\left[(EI)_{eff}^H\frac{\partial^5 w(x,t)}{\partial x^5}-(EI)_{eff}^L\frac{\partial^3 w(x,t)}{\partial x^3}+(K)_{eff}^L\frac{\partial w(x,t)}{\partial x}\right]_{x=0}^{x=L}dt\\&+\int_0^T\frac{\partial\delta w(x,t)}{\partial x}\left[-(EI)_{eff}^H\frac{\partial^4 w(x,t)}{\partial x^4}+(EI)_{eff}^L\frac{\partial^2 w(x,t)}{\partial x^2}\right]_{x=0}^{x=L}dt\\&+\int_0^T\frac{\partial^2\delta w(x,t)}{\partial x^2}\left[(EI)_{eff}^H\frac{\partial^3 w(x,t)}{\partial x^3}\right]_{x=0}^{x=L}dt\end{aligned} \tag{42}$$

The external work (W) in the first variation form of the proposed model is expressed as the sum of the nodal forces ($\mathbf{P}$) and the applied transverse load $(w_z(x,t))$ over the time interval $[0,T]$:

$$\delta W=\int_0^T\left[\int_0^L w_z(x,t)\delta w(x,t)dx\right]dt+\delta\mathbf{U}^T\mathbf{P} \tag{43}$$

where $\mathbf{P}=[P_1\quad P_2\quad P_3\quad P_4\quad P_5\quad P_6]^T$ is the force vector, comprising the nodal forces; and $\mathbf{U}=[U_1\quad U_2\quad U_3\quad U_4\quad U_5\quad U_6]^T$ is the displacement vector, comprising the nodal displacements.

The kinetic energy (K) in the first variation form of the nanobeam, formulated within the MSGET framework over the time interval $[0,T]$, is evaluated by extending the methodology proposed by Demir [66], as expressed below:

$$\delta K=\int_0^T\left[\int_0^L\delta w(x,t)\left[-\rho A\frac{\partial^2 w(x,t)}{\partial t^2}\right]dx\right]dt+\int_0^T\delta w(x,t)\left[\rho A\frac{\partial w(x,t)}{\partial t}\right]_{x=0}^{x=L}dt \tag{44}$$

where ρ is the nanobeam's mass density.

To derive the governing differential equation of motion (GDEM) and its boundary conditions (BCs), Hamilton's principle is employed. Accordingly, Eqs. (42) to (44) can be presented collectively as:

$$\begin{aligned}
&\delta\left\{\int_0^T [\mathrm{K}-(\mathrm{U}-\mathrm{W})]\right\}dt=0\\
&=\int_0^T\int_0^L \delta w(x,t)\left[(EI)_{eff}^{H}\frac{\partial^6 w(x,t)}{\partial x^6}-(EI)_{eff}^{L}\frac{\partial^4 w(x,t)}{\partial x^4}+(K)_{eff}^{L}\frac{\partial^2 w(x,t)}{\partial x^2}-k_{sub}w(x,t)+w_z(x,t)-\rho A\frac{\partial^2 w(x,t)}{\partial t^2}\right]dxdt\\
&+\int_0^T \delta w(x,t)\left[-(EI)_{eff}^{H}\frac{\partial^5 w(x,t)}{\partial x^5}+(EI)_{eff}^{L}\frac{\partial^3 w(x,t)}{\partial x^3}-(K)_{eff}^{L}\frac{\partial w(x,t)}{\partial x}+\rho A\frac{\partial w(x,t)}{\partial t}\right]_{x=0}^{x=L}dt\\
&+\int_0^T \frac{\partial \delta w(x,t)}{\partial x}\left[(EI)_{eff}^{H}\frac{\partial^4 w(x,t)}{\partial x^4}-(EI)_{eff}^{L}\frac{\partial^2 w(x,t)}{\partial x^2}\right]_{x=0}^{x=L}dt\\
&+\int_0^T \frac{\partial^2 \delta w(x,t)}{\partial x^2}\left[-(EI)_{eff}^{H}\frac{\partial^3 w(x,t)}{\partial x^3}\right]_{x=0}^{x=L}dt+\delta\mathbf{U}^{\mathrm{T}}\mathbf{P}=0
\end{aligned}\tag{45}$$

Given the arbitrariness of $\delta w(x,t)$, the GDEM for the proposed model can be expressed as:

$$(EI)_{eff}^{H}\frac{\partial^6 w(x,t)}{\partial x^6}-(EI)_{eff}^{L}\frac{\partial^4 w(x,t)}{\partial x^4}+(K)_{eff}^{L}\frac{\partial^2 w(x,t)}{\partial x^2}-k_{sub}w(x,t)+w_z(x,t)=\rho A\frac{\partial^2 w(x,t)}{\partial t^2}\tag{46}$$

Equation (46) serves as the fundamental expression for analyzing both the static and dynamic characteristics of the proposed beam–substrate model. Moreover, this equation reduces to the GDEM for a local beam on an elastic foundation when the size-scale and surface-energy parameters approach zero [67].

The BCs of the proposed model in the Cartesian coordinate system are derived by considering the arbitrariness of $\delta w(x,t)$ and $\delta\mathbf{U}$ in Eq. (45), analogous to the derivation of the GDEM in Eq. (46):

$$\begin{aligned}
&P_1=-\left[-(EI)_{eff}^{H}\frac{\partial^5 w(x,t)}{\partial x^5}+(EI)_{eff}^{L}\frac{\partial^3 w(x,t)}{\partial x^3}-(K)_{eff}^{L}\frac{\partial w(x,t)}{\partial x}+\rho A\frac{\partial w(x,t)}{\partial t}\right]_{x=0};\\
&P_2=-\left[(EI)_{eff}^{H}\frac{\partial^4 w(x,t)}{\partial x^4}-(EI)_{eff}^{L}\frac{\partial^2 w(x,t)}{\partial x^2}\right]_{x=0};\\
&P_3=-\left[-(EI)_{eff}^{H}\frac{\partial^3 w(x,t)}{\partial x^3}\right]_{x=0};\\
&P_4=\left[-(EI)_{eff}^{H}\frac{\partial^5 w(x,t)}{\partial x^5}+(EI)_{eff}^{L}\frac{\partial^3 w(x,t)}{\partial x^3}-(K)_{eff}^{L}\frac{\partial w(x,t)}{\partial x}+\rho A\frac{\partial w(x,t)}{\partial t}\right]_{x=L};\\
&P_5=\left[(EI)_{eff}^{H}\frac{\partial^4 w(x,t)}{\partial x^4}-(EI)_{eff}^{L}\frac{\partial^2 w(x,t)}{\partial x^2}\right]_{x=L};\\
&P_6=\left[-(EI)_{eff}^{H}\frac{\partial^3 w(x,t)}{\partial x^3}\right]_{x=L}
\end{aligned}\tag{47}$$

6.1. Bending analyses: analytical Solutions

For the bending analysis, the governing differential equation (GDE) of the proposed model is obtained by neglecting the inertia and applied axial forces (*P*). Consequently, Eq. (46) reduces to the following form in the spatial domain *x*:

$$-(EI)_{eff}^{H}\frac{\partial^6 w(x)}{\partial x^6}+(EI)_{eff}^{L}\frac{\partial^4 w(x)}{\partial x^4}-\tau_{res}^{sur}S_{\Gamma}\frac{\partial^2 w(x)}{\partial x^2}+k_{sub}w(x)+w_z(x)=0\tag{48}$$

It can be noted that the form of the GDE in Eq. (48) resembles that of a beam on a three-parameter elastic foundation [68–69]. Therefore, the analytical solutions for such beam systems can be applied here. The general solution of the GDE in Eq. (48) comprises two components:

$$w(x)=w^h(x)+w^p(x)\tag{49}$$

where $w^p(x)$ is the particular solution; and $w^h(x)$ is the homogeneous solution.

The homogeneous solution $(w^h(x))$ of the GDE in Eq. (48) can be generally expressed following the works of Morfidis [68] and Avramidis and Morfidis [69] as:

$$w^h(x)=\varphi_1(x)C_1+\varphi_2(x)C_2+\varphi_3(x)C_3+\varphi_4(x)C_4+\varphi_5(x)C_5+\varphi_6(x)C_6\tag{50}$$

where C_1, C_2, C_3, C_4, C_5, and C_6 are integration constants determined from the BCs; and $\varphi_1(x)$, $\varphi_2(x)$, $\varphi_3(x)$, $\varphi_4(x)$, $\varphi_5(x)$, and $\varphi_6(x)$ are the generalized displacement functions, as detailed in Appendix A. It is important to emphasize that the general solutions presented in Appendix A are valid over the entire beam domain and encompass all variables required for the boundary-value analysis on $x \in [0, L]$.

6.2. Buckling analyses: analytical solution

To define the critical buckling load (P_{cr}), the GDEM in Eq. (46) is employed once again. By neglecting the inertia force and the transverse load $(w_z(x))$, the GDEM reduces to the following form in the spatial domain *x*:

$$-(EI)_{eff}^{H}\frac{\partial^6 w(x)}{\partial x^6}+(EI)_{eff}^{L}\frac{\partial^4 w(x)}{\partial x^4}-(K)_{eff}^{L}\frac{\partial^2 w(x)}{\partial x^2}+k_{sub}w(x)=0 \tag{51}$$

For brevity, the analysis is restricted to the nanobeam–substrate medium system with simple supports. The corresponding classical boundary conditions (CBCs) are specified as follows:

$$w(x)\big|_{x=0}=0 \quad \text{and} \quad w(x)\big|_{x=L}=0 \tag{52}$$

$$M(x)=\left[-(EI)_{eff}^{H}\frac{\partial^4 w(x)}{\partial x^4}+(EI)_{eff}^{L}\frac{\partial^2 w(x)}{\partial x^2}\right]_{x=0}=0 \quad \text{and} \quad M(x)=\left[-(EI)_{eff}^{H}\frac{\partial^4 w(x)}{\partial x^4}+(EI)_{eff}^{L}\frac{\partial^2 w(x)}{\partial x^2}\right]_{x=L}=0 \tag{53}$$

The non-classical boundary conditions (NBCs) are presented by Zhang and Gao [70] for a simply supported nanobeam system as follows:

$$\kappa(x)=\frac{\partial^2 w(x)}{\partial x^2}\bigg|_{x=0}=0 \quad \text{and} \quad \kappa(x)=\frac{\partial^2 w(x)}{\partial x^2}\bigg|_{x=L}=0 \tag{54}$$

Sae-Long et al. [18] derived an analytical expression for the critical buckling load, wherein the displacement field is formulated as follows:

$$w(x)=\bar{C}\sin(\psi x) \tag{55}$$

where $\bar{C}$ denotes the generalized coordinate; and $\psi=\pi/L$.

The critical buckling load (P_{cr}) is obtained by substituting the analytical solution in Eq. (55) and enforcing the non-triviality condition given in Eq. (51), resulting in:

$$P_{cr}=\frac{(EI)_{eff}^{H}\psi^6+(EI)_{eff}^{L}\psi^4+\tau_{res}^{sur}S_{\Gamma}\psi^2+k_{sub}}{\psi^2} \tag{56}$$

Equation (56) can accurately predict the critical buckling load of the local beam-foundation model (P_{cr}^{local}) when both the surface-layer parameters and the material length scale parameters are set to zero. It is important to note that the critical buckling load given in Eq. (56) accounts for all variables involved in the boundary-value analysis on $x\in[0, L]$; however, it is applicable only to the simply supported boundary condition.

6.3. Free-vibration analyses: analytical solution

For the free vibration analysis of the proposed model, Eq. (46) is considered without the axial force (P) and the transverse load $(w_z(x,t))$. Accordingly, the GDEM is reduced to:

$$(EI)_{eff}^{H}\frac{\partial^6 w(x,t)}{\partial x^6}-(EI)_{eff}^{L}\frac{\partial^4 w(x,t)}{\partial x^4}+\tau_{res}^{sur}S_{\Gamma}\frac{\partial^2 w(x,t)}{\partial x^2}-k_{sub}w(x,t)=\rho A\frac{\partial^2 w(x,t)}{\partial t^2} \tag{57}$$

For simplicity, this study focuses exclusively on the nanobeam–substrate medium system with simple supports. The CBCs for this configuration are defined as follows:

$$w(x,t)\big|_{x=0}=0 \quad \text{and} \quad w(x,t)\big|_{x=L}=0 \tag{58}$$

$$M(x,t)=\left[(EI)_{eff}^{H}\frac{\partial^4 w(x,t)}{\partial x^4}-(EI)_{eff}^{L}\frac{\partial^2 w(x,t)}{\partial x^2}\right]_{x=0}=0 \quad \text{and} \quad M(x,t)=\left[(EI)_{eff}^{H}\frac{\partial^4 w(x,t)}{\partial x^4}-(EI)_{eff}^{L}\frac{\partial^2 w(x,t)}{\partial x^2}\right]_{x=L}=0 \tag{59}$$

The NBCs for the simply supported nanobeam system, as proposed by Kong et al. [63] and Akgöz and Civalek [71], are given as follows:

$$\kappa(x,t)=\frac{\partial^2 w(x,t)}{\partial x^2}\bigg|_{x=0}=0 \quad \text{and} \quad \kappa(x,t)=\frac{\partial^2 w(x,t)}{\partial x^2}\bigg|_{x=L}=0 \tag{60}$$

The separation of variables technique is employed to obtain the analytical solution of Eq. (57). The displacement field satisfies all BCs given in Eqs. (58) to (60) and is expressed as [45, 70]:

$$w(x,t)=\sum_{n=1}^{n=\infty}\bar{C}_n\sin(\psi_n x)e^{i\omega_n t} \tag{61}$$

where i denotes the imaginary number; n denotes the vibration mode; $\bar{C}_n$ denotes the Fourier coefficient; ω_n denotes the natural frequency correspond to the n^{th} vibration mode; and $\psi_n=n\pi/L$.

Upon inserting Eq. (61) into Eq. (57), the natural frequency of the n^{th} vibration mode can be derived by imposing the appropriate non-trivial condition $(\bar{C}_n\neq 0)$. The resulting formulation for the n^{th} natural frequency is:

$$\omega_n=\sqrt{\frac{(EI)_{eff}^{H}\psi_n^6+(EI)_{eff}^{L}\psi_n^4+\tau_{res}^{sur}S_{\Gamma}\psi_n^2+k_{sub}}{\rho A}} \tag{62}$$

Table 1. Material parameters of the nanobeam for all simulation cases.

Simulation	Material	E_{xx} (GPa)	μ (GPa)	E_{xx}^{sur} (nN/nm)	τ_{res}^{sur} (nN/nm)	Reference
I	Iron	56.25	22.50	23,000	110	[72, 73]
II	Silver	76	27.74	1.22	0.89	[74]
III	Lead	16	5.71	8	0.63	[75, 76]

It is important to highlight that, by setting the surface parameters and nonlocal parameters to zero, Eq. (62) collapses to the corresponding natural frequency of the local beam-foundation model (ω_n^{local}). Moreover, the natural frequency expression in Eq. (62) differs from that reported for a strain-gradient nanobeam on an elastic substrate in the previous work [18], particularly in the definitions of the lower-order $((EI)_{eff}^{L})$ and higher-order $((EI)_{eff}^{H})$ flexural rigidities, which constitute the primary bending-resistance characteristics in the respective nanobeam models. It is important to note that the natural frequency given in Eq. (62) accounts for all variables involved in the boundary-value analysis on $x \in [0, L]$; however, it is applicable only to the simply supported boundary condition.

7. Numerical Simulations

To analyze the static and dynamic performance of nanobeam–substrate medium systems, three numerical simulations are carried out in this section. The first simulation evaluates the effects of system parameters on bending behavior, the second examines the buckling load, and the third investigates how the natural frequencies vary with system parameters. All simulations were performed in Mathematica [61]. The material properties of the nanobeam used in the simulations are listed in Table 1.

7.1. Simulation I: bending analysis

In this simulation, a cantilever nanobeam-substrate medium system is employed to investigate the impact of system parameters on flexural behavior, as presented in Fig. 4. The nanobeam has a square cross-section with height (h) in nm and a fixed length (L) of 1,000 nm. A concentrated load (P_{end}) of 500 nN is applied at the free end of the nanobeam, while the material length scale parameter (l_0) is maintained at 100 nm. The nanobeam's material properties are provided in Table 1. To study the effects of system parameters on bending behavior, this simulation considers the material length-scale parameters (l_1 and l_2), the non-dimensional substrate modulus ($\bar{K}_{sub} = k_{sub}L^4 / (EI)_{eff}^{L}$), the slenderness ratio (h/L), and the non-dimensional surface parameters ($\tau_{res}^{sur} / E_{xx}^{sur}$). The effective bulk modulus (EBM, E_{bulk}^{eff}) represents the equivalent bulk stiffness of the nanobeam–substrate system, incorporating surface-energy effects to characterize bending behavior. The EBM can be determined using the following equation:

$$v_{end} = \frac{P_{end}\left(\sinh\left(2L\left(k_{sub} / 4E_{bulk}^{eff}I_{xx}\right)^{1/4}\right) - \sin\left(2L\left(k_{sub} / 4E_{bulk}^{eff}I_{xx}\right)^{1/4}\right)\right)}{2E_{bulk}^{eff}I_{xx}\left(k_{sub} / 4E_{bulk}^{eff}I_{xx}\right)^{3/4}\left(2 + \cos\left(2L\left(k_{sub} / 4E_{bulk}^{eff}I_{xx}\right)^{1/4}\right) + \cosh\left(2L\left(k_{sub} / 4E_{bulk}^{eff}I_{xx}\right)^{1/4}\right)\right)} \tag{63}$$

It is worth noting that the end transverse displacement (v_{end}) on the left-hand side of Eq. (63) is calculated through the proposed model, while the terms on the right-hand side are derived based on the classical beam on foundation model [67]. Therefore, the EBM can be obtained by solving the nonlinear relation of this equation, as suggested by Limkatanyu et al. [16].

To examine the impacts of the material length scale parameters (l_1 and l_2) and the non-dimensional substrate modulus ($\bar{K}_{sub}$) on the EBM, the section height (h) is fixed at 100 nm. The material length scale parameters are normalized by and varied from 0 to 2, while the non-dimensional substrate modulus values are set to 1 and 10 [18]. For the material and geometric properties considered, both solution cases ($\Delta = \alpha^3 + \beta^2 > 0$ and $\Delta = \alpha^3 + \beta^2 < 0$) are activated. The analytical results in Fig. 5 show that increasing the material length scale parameters, which represent nonlocal effects, leads to an increase in EBM. Likewise, a higher non-dimensional substrate modulus causes a slight increase in the EBM. Overall, this investigation highlights the influence of substrate–structure interaction and nonlocal effects on the flexural behavior of a nanobeam- substrate medium system.

To analyze the effects of the slenderness ratio (h/L) and the non-dimensional surface parameters ($\tau_{res}^{sur} / E_{xx}^{sur}$) on the EBM, the material length scale parameters (l_1 and l_2) are maintained at a constant value of 100 nm. The non-dimensional surface parameters range from 0.001 to 0.2, while the slenderness ratio is varied between 0.05 and 0.2 [18]. For the material and geometric properties considered, both solution cases ($\Delta = \alpha^3 + \beta^2 > 0$ and $\Delta = \alpha^3 + \beta^2 < 0$) are activated. The analytical results in Fig. 6 indicate that the influence of surface energy on the EBM becomes more pronounced as the slenderness ratio decreases and the non-dimensional surface parameters increase. This behavior results from the higher beam surface-area-to-section-area ratio, consistent with the findings of Sae-Long et al. [18] and Limkatanyu et al. [45]. Additionally, an increase in the non-dimensional substrate modulus ($\bar{K}_{sub}$) produces a slight increase in the EBM. These results underscore the significant role of surface-energy effects in governing the flexural response of a nanobeam on a substrate medium.

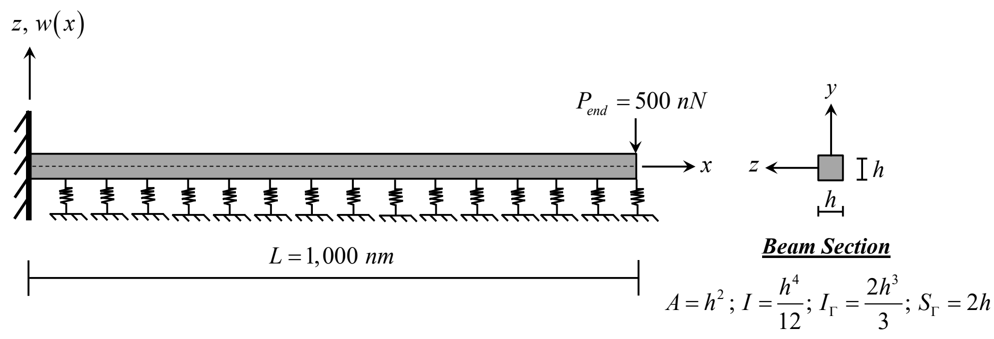

Fig. 4. Simulation I: investigation of the bending characteristics of a cantilever nanobeam on Winkler foundation subjected to an end load P_{end}, including details of its geometry and cross-sectional properties.

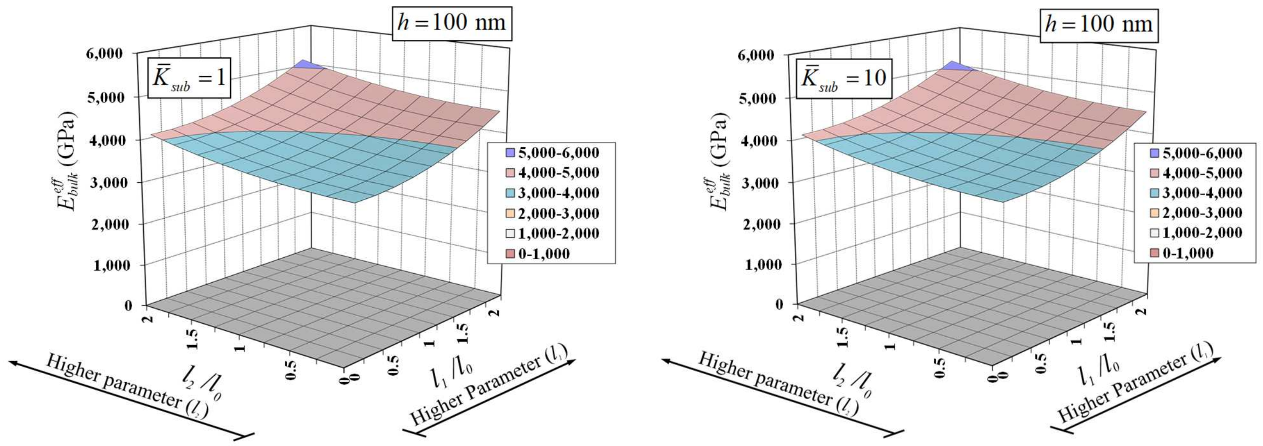

(a) (b)

Fig. 5. Variation of the EBM on the normalized material length scale parameters for: (a) $\bar{K}_{sub} = 1$; and (b) $\bar{K}_{sub} = 10$.

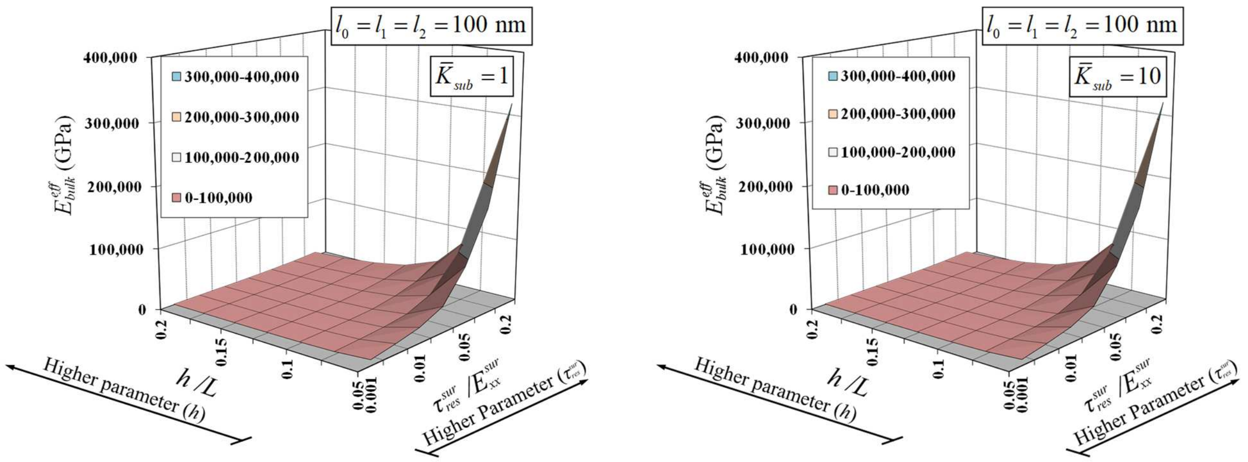

(a) (b)

Fig. 6. Variation of the EBM on the slenderness ratio and non-dimensional surface parameters $\tau_{res}^{sur} / E_{xx}^{sur}$ for: (a) $\bar{K}_{sub} = 1$; and (b) $\bar{K}_{sub} = 10$.

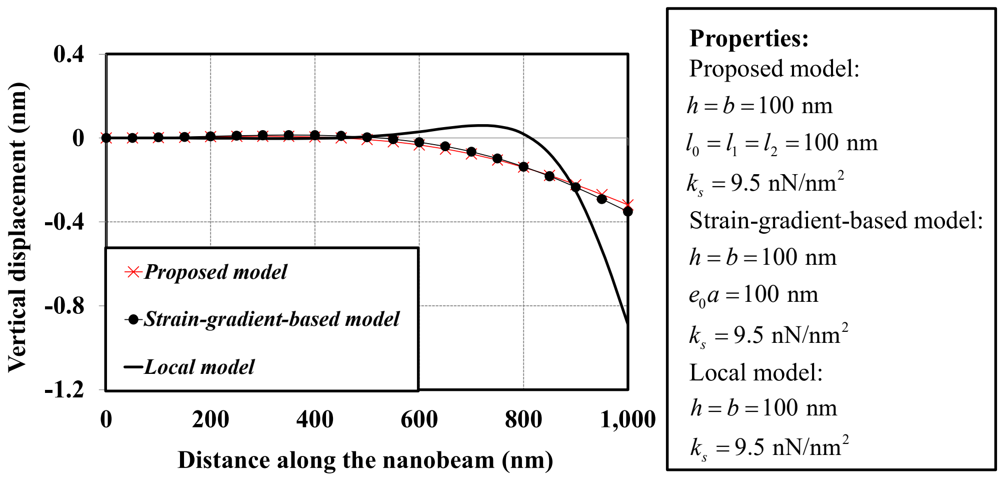

Fig. 7. Bending deflection along the length of the cantilever nanobeam, illustrating the system stiffness induced by size-scale effects and surface energy.

However, it can be observed that the variations in EBM in Figs. 5 and 6 change only slightly with changes in the non-dimensional substrate modulus ($\bar{K}_{sub}$). This is because, within the parameter range considered, EBM is governed primarily by the MSGET-induced higher-order bending-stiffness terms, whereas the foundation contribution enters the EBM identification through Eq. (63) in a comparatively weak manner (notably through the fourth-root dependence on the foundation modulus in the classical beam-on-foundation formulation). Consequently, increasing $\bar{K}_{sub}$ from 1 to 10 produces only a modest shift in the EBM surface compared with the variation induced by the length-scale parameters (Fig. 5) and the surface parameters (Fig. 6).

To highlight the influence of surface energy and nonlocal effects, and to compare the proposed model with existing formulations, Fig. 7 presents the transverse displacement distribution along the nanobeam length. In this work, the nanobeam–substrate system is modeled using a strain-gradient-based formulation derived from the thermodynamics-based strain gradient theory [18]. For comparison, a local model based on classical elasticity is also considered; this model neglects all nonlocal and surface-related effects. The results indicate that incorporating surface energy and nonlocality increases the system stiffness, leading to a reduction in transverse displacement. In addition, the proposed model predicts a higher stiffness than the strain-gradient-based model because it includes extra material length-scale parameters associated with higher-order stresses. The end displacement obtained from the two nonlocal models differs from the local-model prediction by approximately 64.14% and 60.45%, respectively.

7.2. Simulation II: buckling analysis

This simulation employs a simply supported nanobeam, illustrated in Fig. 8, to examine the buckling behavior of the nanobeam-substrate medium system. The nanobeam has a square cross-section with a height of 100 nm and a length of 1,000 nm. As listed in Table 1, the material properties include a fixed material length scale parameter (l_0) of 100 nm. The influence of the length scale parameters $(l_1$ and $l_2)$ and the non-dimensional substrate modulus $(\bar{K}_{sub})$ on the critical buckling load (P_{cr}) in Eq. (56) is explored by varying the normalized length scale parameters from 0 to 2 and selecting values of the substrate modulus $(\bar{K}_{sub})$ between 1 and 10 [18].

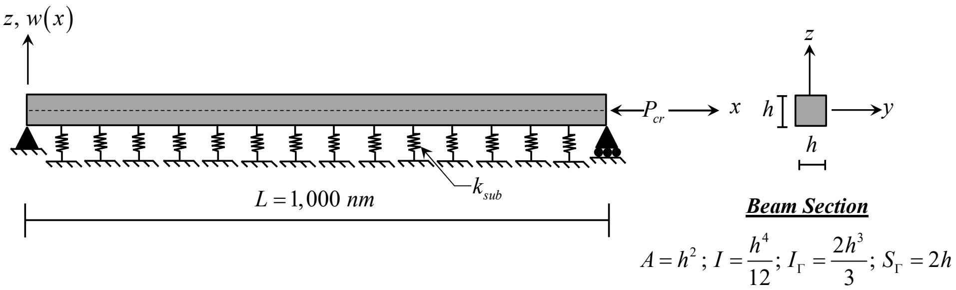

Fig. 8. Simulation II: investigation of the buckling characteristics of a simply supported nanobeam on Winkler foundation, including details of its geometry and cross-sectional properties.

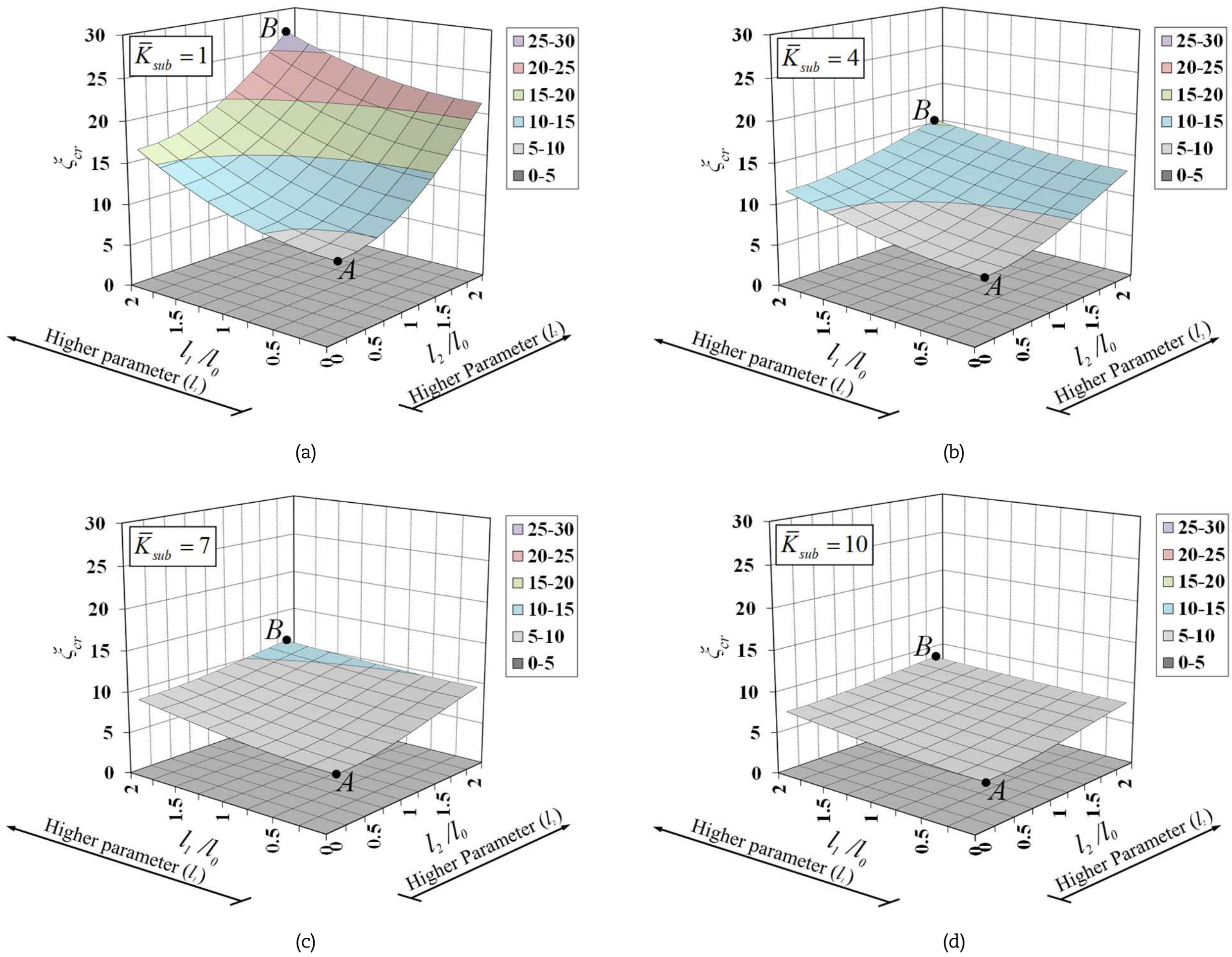

Fig. 9. Influence of normalized material length scale parameters on the normalized critical buckling load P_{cr} for: (a) $\bar{K}_{sub} = 1$; (b) $\bar{K}_{sub} = 4$; (c) $\bar{K}_{sub} = 7$; and (d) $\bar{K}_{sub} = 10$.

The distribution of the normalized critical buckling load $(\xi_{cr} = P_{cr} / P_{cr}^{local})$ with respect to the normalized material length scale parameters $(l_1 / l_0$ and $l_2 / l_0)$, as well as the non-dimensional substrate modulus $(\bar{K}_{sub})$, is presented in Fig. 9. The results show that increasing the material length scale parameters (i.e., enhancing the nonlocal effect) leads to an increase in the normalized critical buckling load, particularly in a softening substrate medium (lower values of $\bar{K}_{sub}$), as indicated at point B. Conversely, a reduction in nonlocality decreases the critical buckling load, as found at point A. In this case study, the surface-energy contribution remains constant and continues to enhance the system stiffness. Collectively, these results demonstrate that the buckling characteristics of the nanobeam–substrate system are governed by the combined effects of substrate–structure interaction, nonlocality, and surface energy, which together enhance the overall system stiffness, consistent with previous findings on the buckling behavior of nanobeams on a Winkler foundation [18, 45].

7.3. Simulation III: free vibration analysis

In the final simulation, parametric analyses are performed to assess the effects of the material length-scale parameters (nonlocal parameters) and substrate modulus on the first natural frequency of the proposed model, as defined in Eq. (62). As shown in Fig. 10, a simply supported nanobeam system resting on an elastic substrate medium is considered. The nanobeam has a square cross-section with a height (h) of 100 nm and a length (L) of 1,000 nm, while the reference nonlocal parameter (l_0) is set to 100 nm. To investigate the variation in natural frequency with respect to the nonlocal parameters and the substrate modulus, the nonlocal parameters $(l_1$ and $l_2)$ are normalized by l_0 over a range of 0 to 2. The non-dimensional substrate modulus $(\bar{K}_{sub})$ is varied from 1 to 10 [18].

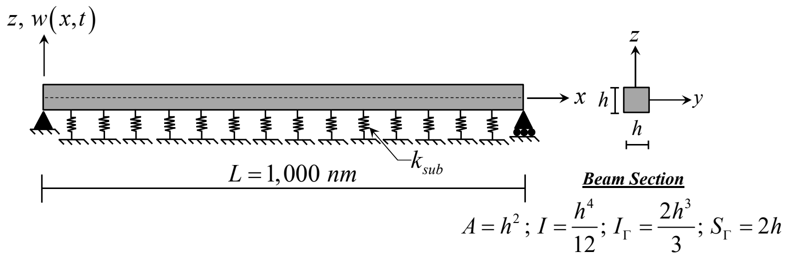

Fig. 10. Simulation III: investigation of the free-vibration characteristics of a simply supported nanobeam on Winkler foundation, including details of its geometry and cross-sectional properties.

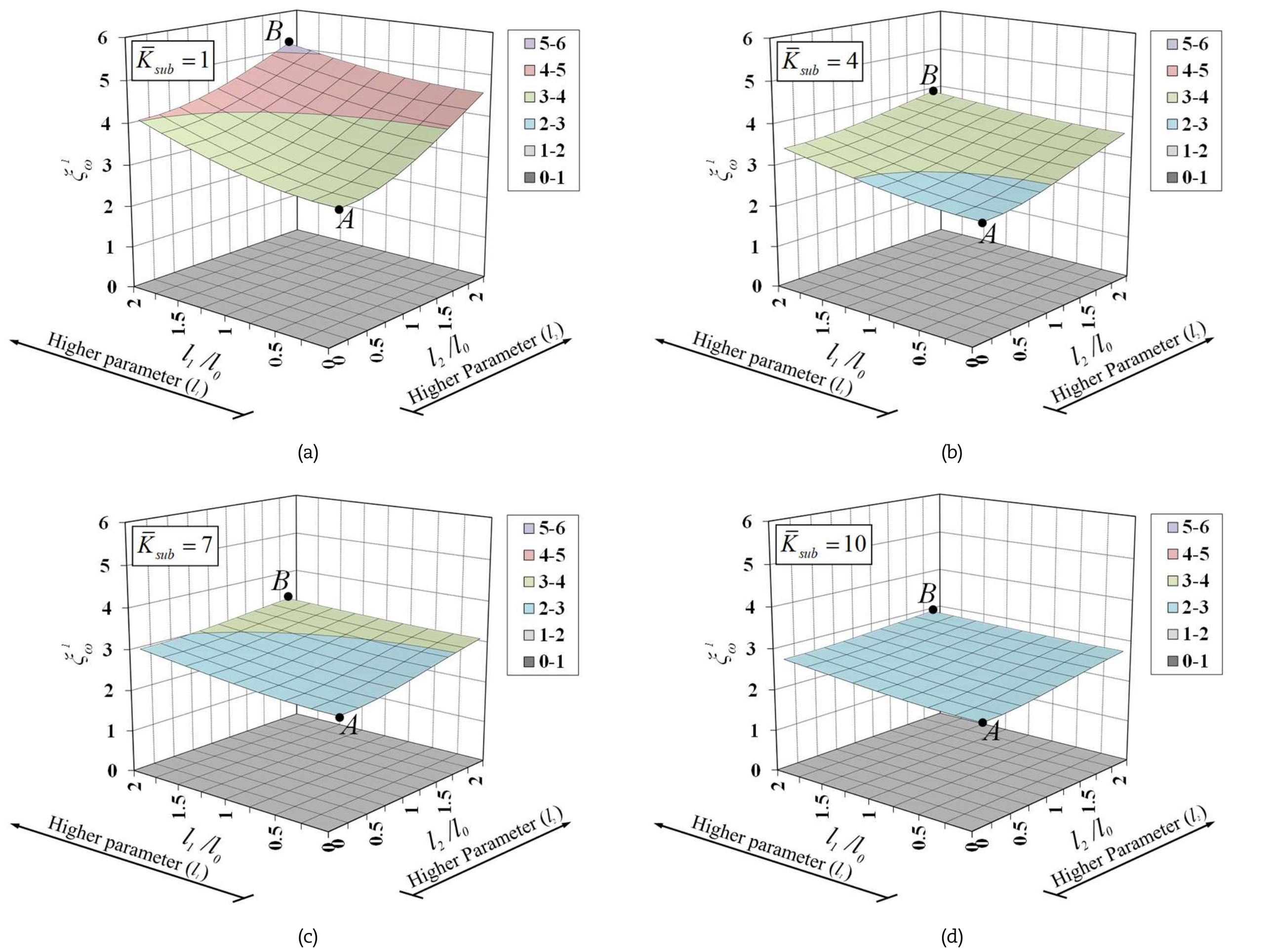

Fig. 11. Influence of normalized material length scale parameters on the normalized first-mode natural frequency ξ_ω^1 for: (a) $\bar{K}_{sub} = 1$; (b) $\bar{K}_{sub} = 4$; (c) $\bar{K}_{sub} = 7$; and (d) $\bar{K}_{sub} = 10$.

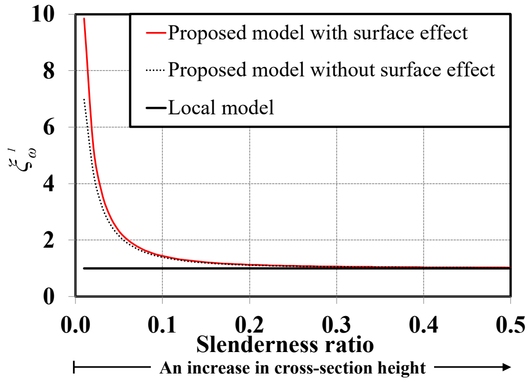

Fig. 12. Increase in natural frequency due to surface-energy-enhanced system stiffness versus slenderness ratio for a simply supported nanobeam on Winkler foundation.

Figure 11 presents the variation of the normalized first-mode natural frequency ($\xi_\omega^1 = \omega_1 / \omega_1^{local}$) with respect to the normalized nonlocal parameters (l_1 / l_0 and l_2 / l_0) and the non-dimensional substrate modulus ($\bar{K}_{sub}$). The analytical results show that a reduction in the material length-scale parameters decreases the degree of nonlocality, leading to a reduction in the normalized natural frequency, as found at point A. In contrast, increasing the nonlocality results in a higher normalized natural frequency, as seen at point B, with the increase being more pronounced for soft substrate media (lower values of $\bar{K}_{sub}$). Furthermore, the surface-energy contributes to rise in system stiffness, thereby enhancing the normalized natural frequency. These results highlight that the interplay among nonlocal effects, surface energy, and substrate–structure interaction is a key factor governing the free-vibration characteristics of nanobeam systems supported by elastic media, consistent with similar trends reported in previous studies [18, 45].

To further clarify the impact of surface energy, the structure system depicted in Fig. 10 was reanalyzed. The slenderness ratio (h / L) was varied from 0.01 to 0.5 while maintaining a constant beam length of 1,000 nm. The nonlocal parameters (l_0, l_1, and l_2) were fixed at 25 nm, and the non-dimensional substrate modulus ($\bar{K}_{sub}$) was set to 1. To compare the normalized first-mode natural frequency ($\xi_\omega^1 = \omega_1 / \omega_1^{local}$), three analytical models were employed: the proposed model with surface effects, the proposed model without surface effects, and the classical local model. Figure 12 shows that surface energy enhances system stiffness—especially for small slenderness ratios—resulting in higher normalized natural frequencies. Nonetheless, comparison with the local model reveals that nonlocal effects dominate over surface-energy contributions.

Across the three numerical simulations, the results identify three practically relevant dominance regimes: (i) Surface-dominant regime—for small h / L and/or large $\tau_{res}^{sur} / E_{xx}^{sur}$, surface energy markedly increases the effective stiffness, thereby increasing E_{bulk}^{eff}, P_{cr}, and ω_n. (ii) Nonlocal (MSGET)-dominant regime—for large normalized length-scale parameters l_1 / l_0 and l_2 / l_0, strain-gradient effects significantly stiffen the response, particularly on soft substrates. (iii) Foundation-dominant regime—for sufficiently large $\bar{K}_{sub}$, substrate interaction becomes the primary contributor to overall stiffness; however, within the present parameter ranges its influence is weaker than that of the surface and MSGET parameters, which explains the small differences observed in Figs. 5 and 6.

8. Conclusions

This paper introduces a refined analytical model for investigating the static and dynamic behavior of nanobeams supported by an elastic substrate. A distinguishing feature of the proposed formulation is the explicit incorporation of surface-energy effects. The model integrates the modified strain gradient elasticity theory (MSGET) with the Euler–Bernoulli beam theory (EBBT) to account for nonlocal mechanics, while the interaction with the substrate is represented using the Winkler foundation model. The Gurtin–Murdoch surface elasticity theory is employed to capture size-dependent influences at the nanoscale. Hamilton's principle is utilized to derive the governing differential equations and boundary conditions. Three numerical case studies are carried out to assess the system's static and dynamic performance. The major conclusions are as follows:

- Increasing the material length-scale parameters and substrate modulus enhances the effective bulk modulus (EBM).
- A lower slenderness ratio and higher non-dimensional surface parameters ($\tau_{res}^{sur} / E_{xx}^{sur}$) also lead to an increase in EBM.
- The proposed model exhibits the highest system stiffness compared with both strain-gradient-based and classical local models in bending analysis.
- Increasing the nonlocal effects result in higher normalized critical buckling loads and normalized natural frequencies, particularly for systems on soft substrate media.
- Surface-energy effects consistently contribute to stiffness enhancement.
- The interaction among substrate–structure coupling, surface energy, and nonlocality plays a crucial role in the free vibration, buckling, and flexural responses of nanobeam-substrate systems.

The proposed closed-form framework can aid the design and interpretation of nanobeam-based devices interacting with compliant substrates, including nanoresonators, AFM cantilevers operating near surfaces, nanowires/CNTs embedded in polymer matrices, and stretchable or flexible electronic components. Future work may extend the formulation to shear-deformable kinematics (Timoshenko beams), two-parameter or viscoelastic foundations (e.g., Pasternak or Kelvin–Voigt media), geometric and/or material nonlinearities, and multiphysics couplings (thermal, piezoelectric, or flexoelectric effects).

Author Contributions

W. Sae-Long played a role in conceptualization, methodology, software, validation, formal analysis, investigation, data curation, writing and revising the manuscript, visualization, supervision, project administration, and funding acquisition; S. Limkatanyu played a role in methodology, software, formal analysis, investigation, writing and revising the manuscript, and supervision; P. Sukontasukkul was responsible for formal analysis, investigation, supervision, and funding acquisition; J. Rungamornrat

implemented the formal analysis, investigation, data curation, and supervision; S. Keawsawasvong played a role in investigation and supervision; T. Chompoorat contributed to investigation, supervision, and funding acquisition; P. Chaimahawan played roles in investigation and supervision; A. Pimanmas played roles in investigation and supervision; The manuscript was written through the contribution of all authors. All authors discussed the results, reviewed, and approved the final version of the manuscript.

Acknowledgments

Not applicable.

Conflict of Interest

The authors declared no potential conflicts of interest concerning the research, authorship, and publication of this article.

Funding

This study was financially supported by University of Phayao and Thailand Science Research and Innovation Fund (Fundamental Fund 2026, Grant No. 2406/2568) awarded to W. Sae-Long, by National Research Council of Thailand (NRCT) under the Senior Research Scholar program (Contract No. N42A690479) awarded to P. Sukontasukkul, and by Thailand Science Research and Innovation Fund and the University of Phayao (FF69, Grant No. 2286/2568) awarded to T. Chompoorat.

Data Availability Statements

The datasets generated and/or analyzed during the current study are available from the corresponding author on reasonable request.

References

[1] Agbogo, V.U., Sadiku, E.R., Mavhungu, L., Kupolati, W.K., Injor, O.M., Nanotechnology coatings in the defense and aerospace industry, *Next Nanotechnology*, 7, 2025, 100197.
[2] Hanmante, P.S., Lohiya, R.T., Wankhede, A.G., Undirwade, D.S., Lade, S.N., Burle, S.S., Umekar, M.J., Quantum dot nanotechnology: Advancing target drug delivery in Oncology, *Next Nanotechnology*, 7, 2025, 100172.
[3] Sae-Long, W., Limkatanyu, S., Prachasaree, W., Rungamornrat, J., Sukontasukkul, P., A thermodynamics-based nonlocal bar-elastic substrate model with inclusion of surface-energy effect, *Journal of Nanomaterials*, 2020, 8276745.
[4] Ghafoorian, F., Wan, H., Chegini, S., A systematic analysis of a small-scale HAWT configuration and aerodynamic performance optimization through kriging, factorial, and RSM methods, *Journal of Applied and Computational Mechanics*, 11(4), 2025, 887-903.
[5] Murti, B.T., Putri, A.D., Izati, M., Sulaekhah, M., Yang, P.-K., Electrochemical and colorimetric nano(bio)sensors for point-of-care detection of creatinine, *Next Nanotechnology*, 8, 2025, 100314.
[6] Lee, S.H., A 3D-printed microcantilever holder for atomic force microscopes using a mounted microcantilever, *International Journal of Precision Engineering and Manufacturing*, 24, 2023, 303-307.
[7] Lam, D.C.C., Yang, F., Chong, A.C.M., Wang, J., Tong, P., Experiments and theory in strain gradient elasticity, *Journal of the Mechanics and Physics of Solids*, 51(8), 2003, 1477-1508.
[8] Tang, C., Alici, G., Evaluation of length-scale effects for mechanical behaviour of micro- and nanocantilevers: II. Experimental verification of deflection models using atomic force microscopy, *Journal of Physics D: Applied Physics*, 44(33), 2011, 335502.
[9] Limkatanyu, S., Damrongwiriyanupap, N., Prachasaree, W., Sae-Long, W., Modeling of axially loaded nanowires embedded in elastic substrate media with inclusion of nonlocal and surface effects, *Journal of Nanomaterials*, 2013, 2013, 635428.
[10] Farazin, A., Aghadavoudi, F., Motififard, M., Saber-Samandari, S., Khandan, A., Nanostructure, molecular dynamics simulation and mechanical performance of PCL membranes reinforced with antibacterial nanoparticles, *Journal of Applied and Computational Mechanics*, 7(4), 2021, 1907-1915.
[11] Limkatanyu, S., Sae-Long, W., Mohammad-Sedighi, H., Rungamornrat, J., Sukontasukkul, P., Imjai, T., Zhang, H., Static and free vibration analyses of single-walled carbon nanotube (SWCNT)-substrate medium systems, *Nanomaterials*, 12(10), 2022, 1740.
[12] Barretta, R., Canadija, M., Marotti de Sciarra, F., Skoblar, A., Free vibrations of Bernoulli-Euler nanobeams with point mass interacting with heavy fluid using nonlocal elasticity, *Nanomaterials*, 12(15), 2022, 2676.
[13] Barretta, R., Luciano, R., Marotti de Sciarra, F., Vaccaro, M.S., Modelling issues and advances in nonlocal beams mechanics, *International Journal of Engineering Science*, 198, 2024, 104042.
[14] Xu, D., Wang, Z., Chen, L., Thaiyanurak, T., Atomic mechanisms of crystallization in nano-sized metallic glasses, *Crystals*, 13(1), 2023, 32.
[15] Jena, S.S., Singh, S., Chandra, S., Characterizing MRO in atomistic models of vitreous SiO2 generated using ab-initio molecular dynamics, *Applied Physics A*, 129, 2023, 742.
[16] Limkatanyu, S., Sae-Long, W., Horpibulsuk, S., Prachasaree, W., Damrongwiriyanupap, N., Flexural responses of nanobeams with coupled effects of nonlocality and surface energy, *ZAMM – Journal of Applied Mathematics and Mechanics*, 98(10), 2018, 1771-1793.
[17] Barretta, R., Fabbrocino, F., Luciano, R., Marotti de Sciarra, F., Closed-form solutions in stress-driven two-phase integral elasticity for bending of functionally graded nano-beams, *Physica E: Low-dimensional Systems and Nanostructures*, 97, 2018, 13-30.
[18] Sae-Long, W., Limkatanyu, S., Rungamornrat, J., Prachasaree, W., Sukontasukkul, P., Sedighi, H.M., A rational beam-elastic substrate model with incorporation of beam-bulk nonlocality and surface-free energy, *The European Physical Journal Plus*, 136, 2021, 80.
[19] Mojahedi, M., Analytical and numerical investigation of a nonlinear nanobeam model, *Journal of Vibration Engineering & Technologies*, 12, 2024, 3471-3485.
[20] Wagner, G.J., Liu, W.K., Coupling of atomistic and continuum simulations using a bridging scale decomposition, *Journal of Computational Physics*, 190(1), 2003, 249-274.
[21] Poluektov, M., Eriksson, O., Kreiss, G., Coupling atomistic and continuum modelling of magnetism, *Computer Methods in Applied Mechanics and Engineering*, 329, 2018, 219-253.
[22] Sae-Long, W., Limkatanyu, S., Sukontasukkul, P., Damrongwiriyanupap, N., Rungamornrat, J., Prachasaree, W., Fourth-order strain gradient bar-substrate model with nonlocal and surface effects for the analysis of nanowires embedded in substrate media, *Facta Universitatis, Series: Mechanical Engineering*, 19(4), 2021, 657-680.
[23] Abouelregal, A.E., Marin, M., Askar, S.S., Analysis of the magneto-thermoelastic vibrations of rotating Euler–Bernoulli nanobeams using the nonlocal elasticity model, *Boundary Value Problems*, 2023, 2023, 21.
[24] Caporale, A., Luciano, R., Scorza, D., Vantadori, S., Local–nonlocal stress-driven model for multi-cracked nanobeams, *International Journal of Solids and Structures*, 273, 2023, 112230.
[25] Ahmadi, I., Moradi, M.N., Panah, M.D., Dynamic response analysis of nanoparticle-nanobeam impact using nonlocal theory and meshless method, *Structural Engineering and Mechanics*, 89(2), 2024, 135-153.
[26] Ghoytasi, I., Naghdabadi, R., Small-scale effects on wave propagation in curved nanobeams subjected to thermal loadings based on NSGT, *Advances in nano research*, 16(2), 2024, 187-200.
[27] Liu, Z., Zhou, Z., Static and free vibration responses of nanobeams considering flexoelectricity and surface effect, *AIP Advances*, 14, 2024, 035340.
[28] Srivastava, A., Mukhopadhyay, S., Damping analysis of a transversely isotropic piezothermoelastic nanobeam resonator based on the MGT thermoelasticity, *European Journal of Mechanics - A/Solids*, 106, 2024, 105327.
[29] Civalek, Ö., Uzun, B., Yaylı, M.Ö., On the stability analysis of a restrained FG nanobeam in an elastic matrix with neutral axis effects, *Zeitschrift für Naturforschung A*, 79(7), 2024, 735-753.
[30] Jena, S.K., Pradyumna, S., Chakraverty, S., Quantifying uncertainty in free vibration characteristics of nanobeam with one variable first-order shear deformation theory: an analytical investigation, *Acta Mechanica*, 235, 2024, 4401-4416.

[31] Movassagh, A.A., Mahmoodi, M.J., A micro-scale modeling of Kirchhoff plate based on modified strain-gradient elasticity theory, *European Journal of Mechanics - A/Solids*, 40, 2013, 50-59.
[32] Ansari, R., Gholami, R., Size-dependent vibration of functionally graded curved microbeams based on the modified strain gradient elasticity theory, *Archive of Applied Mechanics*, 83, 2013, 1439-1449.
[33] Ansari, R., Gholami, R., Shojaei, M.F., Mohammadi, V., Sahmani, S., Bending, buckling and free vibration analysis of size-dependent functionally graded circular/annular microplates based on the modified strain gradient elasticity theory, *European Journal of Mechanics - A/Solids*, 49, 2015, 251-267.
[34] Salehipour, H., Shahsavar, A., A three dimensional elasticity model for free vibration analysis of functionally graded micro/nano plates: Modified strain gradient theory, *Composite Structures*, 206, 2018, 415-424.
[35] Thai, S., Thai, H.-T., Vo, T.P., Patel, V.I., Size-dependant behaviour of functionally graded microplates based on the modified strain gradient elasticity theory and isogeometric analysis, *Computers & Structures*, 190, 2017, 219-241.
[36] Bostani, M., Mohammadi, A.K., Thermoelastic damping in microbeam resonators based on modified strain gradient elasticity and generalized thermoelasticity theories, *Acta Mechanica*, 229, 2018, 173-192.
[37] Su, L., Sahmani, S., Safaei, B., Modified strain gradient-based nonlinear building sustainability of porous functionally graded composite microplates with and without cutouts using IGA, *Engineering with Computers*, 39, 2023, 2147-2167.
[38] Chu, J., Wang, Y., Sahmani, S., Safaei, B., Nonlinear large-amplitude oscillations of PFG composite rectangular microplates based upon the modified strain gradient elasticity theory, *International Journal of Structural Stability and Dynamics*, 22(6), 2022, 2250068.
[39] Gurtin, M.E., Murdoch, A.I., A continuum theory of elastic material surfaces, *Archive for Rational Mechanics and Analysis*, 57, 1975, 291-323.
[40] Gurtin, M.E., Murdoch, A.I., Surface stress in solids, *International Journal of Solids and Structures*, 14(6), 1978, 431-440.
[41] Cammarata, R.C., Surface and interface stress effects in thin films, *Progress in Surface Science*, 46(1), 1994, 1-38.
[42] Juntarasaid, C., Pulngern, T., Chucheepsakul, S., Bending and buckling of nanowires including the effects of surface stress and nonlocal elasticity, *Physica E: Low-dimensional Systems and Nanostructures*, 46, 2012, 68-76.
[43] Nazarenko, L., Bargmann, S., Stolarski, H., Closed-form formulas for the effective properties of random particulate nanocomposites with complete Gurtin–Murdoch model of material surfaces, *Continuum Mechanics and Thermodynamics*, 29, 2017, 77-96.
[44] Lu, P., Liu, R., Zhai, H., Wang, G., Yu, P., Lu, C., A modified beam model based on Gurtin–Murdoch surface elasticity theory, *Meccanica*, 56, 2021, 1147-1164.
[45] Limkatanyu, S., Sae-Long, W., Rungamornrat, J., Buachart, C., Sukontasukkul, P., Keawsawasvong, S., Chindaprasirt, P., Bending, buckling and free vibration analyses of nanobeam-substrate medium systems, *Facta Universitatis, Series: Mechanical Engineering,* 20(3), 2022, 561-587.
[46] Limkatanyu, S., Sae-Long, W., Sedighi, H.M., Rungamornrat, J., Sukontasukkul, P., Prachasaree, W., Imjai, T., Strain-gradient bar-elastic substrate model with surface-energy effect: Virtual-force approach, *Nanomaterials*, 12(3), 2022, 375.
[47] Grekov, M.A., Vakaeva, A.B., Müller, W.H., Stress field around cylindrical nanopore by various models of surface elasticity, *Continuum Mechanics and Thermodynamics*, 35, 2023, 231-243.
[48] Li, P., Li, W., Tan, Y., Fan, H., Wang, Q., A phase field fracture model for ultra-thin micro-/nano-films with surface effects, *International Journal of Engineering Science*, 195, 2024, 104004.
[49] Tiedje, T., Bräuer, C., Luniak, M., Nieweglowski, K., Bock, K., Stereolithographic process for embedding of electronic components into multi-material flexible and stretchable polymer substrate to reduce stress during stretching, *IMAPSource Proceedings*, 2023, 234-238.
[50] Li, J., Meng, X., Shen, Y., Gu, J., Luo, G., Bai, K., Li, H., Xue, Z., Design strategy of porous elastomer substrate and encapsulation for inorganic stretchable electronics, *International Journal of Smart and Nano Materials*, 15(2), 2024, 330-347.
[51] Radhakrishnan, G., Kim, K., Droopad, R., Goyal, A., Heteroepitaxial GaAs thin-films on flexible, large-area, single-crystal-like substrates for wide-ranging optoelectronic applications, *Scientific Reports*, 14, 2024, 10116.
[52] Shen, H.-S., Huang, X.-H., Yang, J., Nonlinear bending of temperature-dependent FG-CNTRC laminated plates with negative Poisson's ratio, *Mechanics of Advanced Materials and Structures*, 27(13), 2020, 1141-1153.
[53] Meng, Z., Guo, L., Huang, B., Ren, S., Xiao, S., Concurrent topology optimization design for CNT orientation and CNTRC layout, *Applied Mathematical Modelling*, 122, 2023, 22-41.
[54] Barretta, R., Marotti de Sciarra, F., A nonlocal model for carbon nanotubes under axial loads, *Advances in Materials Science and Engineering*, 2013, 360935.
[55] Rezaee, M., Hamidi, B.A., Influence of third-order elastic modulus as material nonlinearity on free and forced vibration of a nonlocal nanobeam rested on viscoelastic medium, *Waves in Random and Complex Media*, 2022.
[56] Mamu, R.M., Togun, N., Thermal effects on nonlinear vibration of nonlocal nanobeam embedded in nonlinear elastic medium, *Acta Mechanica*, 2024.
[57] Zhang, Y., Pang, M., Fan, L., Analyses of transverse vibrations of axially pretensioned viscoelastic nanobeams with small size and surface effects, *Physics Letters A*, 380(29-30), 2016, 2294-2299.
[58] Uzun, B., Yaylı, M.Ö., Stability analysis of arbitrary restrained nanobeam embedded in an elastic medium via nonlocal strain gradient theory, *The Journal of Strain Analysis for Engineering Design*, 58(8), 2023, 672-683.
[59] Limkatanyu, S., Sae-Long, W., Rungamornrat, J., Damrongwiriyanupap, N., Keawsawasvong, S., Sukontasukkul, P., Hansapinyo, C., Static bending analysis of nanobeam-substrate medium systems incorporating mixture stress-driven nonlocality, surface energy, and substrate-structure interactions, *Journal of Applied and Computational Mechanics*, 11(2), 2025, 327-343.
[60] Winkler, E., *Die Lehre von der Elastizität und Festigkeit*, Dominicus, Prague, Czechoslovakia, 1867.
[61] Wolfram, S., *Mathematica reference guide*, Addison-Wesley Publishing Company, Redwood City, California, USA, 1992.
[62] Öchsner, A., *Classical beam theories of structural mechanics*, Springer Cham, Switzerland, 2021.
[63] Kong, S., Zhou, S., Nie, Z., Wang, K., Static and dynamic analysis of micro beams based on strain gradient elasticity theory, *International Journal of Engineering Science*, 47(4), 2009, 487-498.
[64] Miller, R.E., Shenoy, V.B., Size-dependent elastic properties of nanosized structural elements, *Nanotechnology*, 11(3), 2000, 139-147.
[65] Gao, X.-L., Mahmoud, F.F., A new Bernoulli–Euler beam model incorporating microstructure and surface energy effects, *Zeitschrift für Angewandte Mathematik und Physik*, 65, 2014, 393-404.
[66] Demir, Ç., Nonlocal vibration analysis for micro/nano beam on Winkler foundation via DTM, *International Journal of Engineering and Applied Sciences*, 8(4), 2016, 108-118.
[67] Limkatanyu, S., Sae-Long, W., Prachasaree, W., Kwon, M., Improved nonlinear displacement-based beam element on a two-parameter foundation, *European Journal of Environmental and Civil Engineering*, 19(6), 2015, 649-671.
[68] Morfidis, K., *Research and development of methods for the modeling of foundation structural elements and soil*, PhD dissertation, Department of Civil Engineering, Aristotle University of Thessaloniki, 2003.
[69] Avramidis, I.E., Morfidis, K., Bending of beams on three-parameter elastic foundation, *International Journal of Solids and Structures*, 43(2), 2006, 357-375.
[70] Zhang, G.Y., Gao, X.-L., A new Bernoulli–Euler beam model based on a reformulated strain gradient elasticity theory, *Mathematics and Mechanics of Solids*, 25(3), 2020, 630-643.
[71] Akgöz, B., Civalek, Ö., Analysis of micro-sized beams for various boundary conditions based on the strain gradient elasticity theory, *Archive of Applied Mechanics*, 82, 2012, 423-443.
[72] Lim, C.W., He, L.H., Size-dependent nonlinear response of thin elastic films with nano-scale thickness, *International Journal of Mechanical Sciences*, 46(11), 2004, 1715-1726.
[73] Mahmoud, F.F., Eltaher, M.A., Static analysis of nanobeams including surface effects by nonlocal finite element, *Journal of Mechanical Science and Technology*, 26, 2012, 3555-3563.
[74] He, J., Lilley, C.M., Surface effect on the elastic behavior of static bending nanowires, *Nano Letters*, 8(7), 2008, 1798-1802.
[75] Cuenot, S., Frétigny, C., Champagne, S.D., Nysten, B., Surface tension effect on the mechanical properties of nanomaterials measured by atomic force microscopy, *Physical Review B*, 69, 2004, 165410.
[76] Wan, J., Fan, Y.L., Gong, D.W., Shen, S.G., Fan, X.Q., Surface relaxation and stress of fcc metals: Cu, Ag, Au, Ni, Pd, Pt, Al and Pb, *Modelling and Simulation in Materials Science and Engineering*, 7(2), 1999, 189-206.

Appendix A

For bending analyses of Eqs. (48), we can express the general form as follows:

$$\frac{d^6 w(x)}{dx^6} + \Omega_1 \frac{d^4 w(x)}{dx^6} + \Omega_2 \frac{d^2 w(x)}{dx^2} + \Omega_3 w(x) = 0 \tag{A1}$$

Parameters Ω_1, Ω_2, and Ω_3 in Eq. (A1) can be defined as:

$$\Omega_1 = -\frac{(EI)_{eff}^{L}}{(EI)_{eff}^{H}};\ \Omega_2 = \frac{\tau_{res}^{sur} S_\Gamma}{(EI)_{eff}^{H}};\text{ and }\Omega_3 = -\frac{k_{sub}}{(EI)_{eff}^{H}} \tag{A2}$$

For reasons of simplicity, the parameters Ω_1, Ω_2, and Ω_3 in Eq. (A2) are restated using the auxiliary parameters for the general solution expression:

$$\Delta = \alpha^3 + \beta^2;\ \alpha = \frac{-\left(\Omega_1^2/3\right) + \Omega_2}{3};\text{ and }\beta = \frac{\left(2\Omega_1^3/27\right) - \left(\Omega_1\Omega_2/3\right) + \Omega_3}{2} \tag{A3}$$

The analytical solution of Eq. (A1) can be expressed in the general form as follows:

$$w^h(x) = \varphi_1(x)C_1 + \varphi_2(x)C_2 + \varphi_3(x)C_3 + \varphi_4(x)C_4 + \varphi_5(x)C_5 + \varphi_6(x)C_6 \tag{A4}$$

According to the solution methods [68, 69], two analytical expressions that depend on the parameter are given by:
- **Solution Case I:** when $\Delta = \alpha^3 + \beta^2 > 0$:

$$\begin{aligned} &\varphi_1(x) = e^{R_1 x}; && \varphi_2(x) = e^{-R_1 x}; && \varphi_3(x) = e^{Rx}\cos[Qx]; \\ &\varphi_4(x) = e^{Rx}\sin[Qx]; && \varphi_5(x) = e^{-Rx}\cos[Qx]; && \varphi_6(x) = e^{-Rx}\sin[Qx] \end{aligned} \tag{A5}$$

where

$$\begin{aligned} &R_1 = \sqrt{\sqrt[3]{-\beta+\sqrt{\Delta}} + \sqrt[3]{-\beta-\sqrt{\Delta}} - \frac{\Omega_1}{3}};\ R = \sqrt{\frac{\left(\sqrt{m^2+n^2}+m\right)}{2}};\ Q = \sqrt{\frac{\left(\sqrt{m^2+n^2}-m\right)}{2}} \\ &m = -\frac{\left[\sqrt[3]{-\beta+\sqrt{\Delta}} + \sqrt[3]{-\beta-\sqrt{\Delta}} + (2\Omega_1/3)\right]}{2};\ n = \frac{\sqrt{3}\left[\sqrt[3]{-\beta+\sqrt{\Delta}} - \sqrt[3]{-\beta-\sqrt{\Delta}}\right]}{2} \end{aligned} \tag{A6}$$

- **Solution Case II:** when $\Delta = \alpha^3 + \beta^2 < 0$:

$$\varphi_1(x) = e^{Rx};\ \varphi_2(x) = e^{-Rx};\ \varphi_3(x) = e^{R_1 x};\ \varphi_4(x) = e^{R_2 x};\ \varphi_5(x) = e^{-R_1 x};\ \varphi_6(x) = e^{-R_2 x} \tag{A7}$$

where

$$\begin{aligned} &R = \sqrt{2\sqrt{-\alpha}\cos\left[\frac{\varphi}{3}\right] - \frac{\Omega_1}{3}};\ R_1 = \sqrt{2\sqrt{-\alpha}\cos\left[\frac{\varphi+2\pi}{3}\right] - \frac{\Omega_1}{3}}; \\ &R_2 = \sqrt{2\sqrt{-\alpha}\cos\left[\frac{\varphi+4\pi}{3}\right] - \frac{\Omega_1}{3}};\ \varphi = \cos^{-1}\left[-\beta/\sqrt{-\alpha^3}\right] \end{aligned} \tag{A8}$$

ORCID iD

Worathep Sae-Long https://orcid.org/0000-0001-8149-4409
Suchart Limkatanyu https://orcid.org/0000-0002-4343-7654
Piti Sukontasukkul https://orcid.org/0000-0002-9580-7063
Jaroon Rungamornrat https://orcid.org/0000-0002-2449-9067
Suraparb Keawsawasvong https://orcid.org/0000-0002-1760-9838
Thanakorn Chompoorat https://orcid.org/0000-0002-5661-1885
Preeda Chaimahawan https://orcid.org/0000-0002-3515-0506
Amorn Pimanmas https://orcid.org/0000-0001-9543-2700

How to cite this article: Sae-Long W., et al., Nonlocal Static and Dynamic Characterization of Nanobeams on Elastic Substrates with Surface Energy Effects, *J. Appl. Comput. Mech.*, 12(3), 2026, 1217-1232. https://doi.org/10.22055/jacm.2026.48980.5640